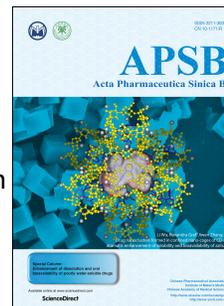# Accepted Manuscript

Direct interaction of DNMT inhibitors to PrP^C suppresses pathogenic process of prion

Dae-Hwan Kim, Chunyan Ren, Chongsuk Ryou, Jiaojie Li

Please cite this article as: Kim D-H, Ren C, Ryou C, Li J, Direct interaction of DNMT inhibitors to PrP^C suppresses pathogenic process of prion, *Acta Pharmaceutica Sinica B*, https://doi.org/10.1016/j.apsb.2019.04.001.

GA
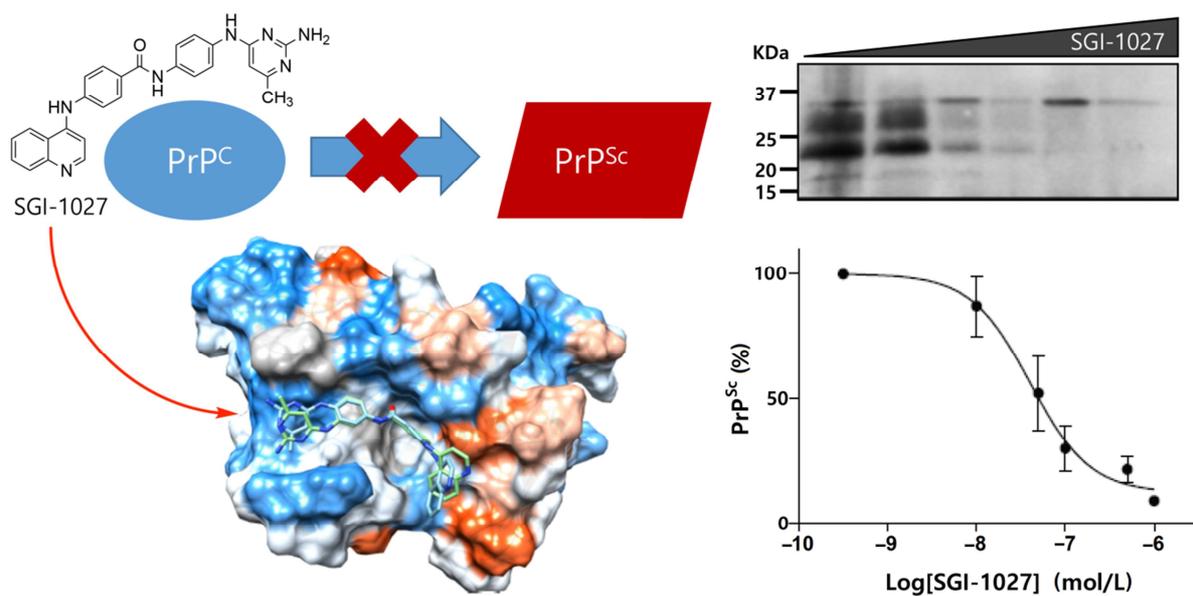
A novel activity of DNMT inhibitor SGI-1027 suppresses the pathogenic process of prion. The direct binding of SGI-1027 to prion protein with a normal conformation suppresses the formation of misfolded prion proteins.

Original Article

Direct interaction of DNMT inhibitors to PrP^C suppresses pathogenic process of prion

Dae-Hwan Kim[a,b]**, Chunyan Ren**[c]**, Chongsuk Ryou**[a,d,**]**, Jiaojie Li**[e,*]

[a]*Institute of Pharmaceutical Science and Technology, Hanyang University, Ansan 15588, Republic of Korea*

[b]*School of Undergraduate Studies, College of Transdisciplinary Studies, Daegu Gyeongbuk Institute of Science and Technology, Daegu 42988, Republic of Korea*

[c]*Boston Children's Hospital, Harvard Medical School, Boston, MA 02115, USA*

[d]*Department of Pharmacy, Hanyang University, Ansan 15588, Republic of Korea*

[e]*Department of Chemistry, Gwangju Institute of Science and Technology, Gwangju 61005, Republic of Korea*

*Corresponding author. Tel.: +82 627153655; fax: +82 627153609.

**Corresponding author. Tel.: +82 314005811; fax: +82 314005958.

E-mail addresses: jjli@gist.ac.kr (Jiaojie Li), cryou2@hanyang.ac.kr (Chongsuk Ryou).

Running title: Direct interaction of DNMT inhibitors to PrP^C suppresses pathogenic process of prion

Abstract The conversion of the normal cellular prion protein (PrP^C) to the misfolded pathogenic scrapie prion protein (PrP^{Sc}) is the biochemical hallmark of prion replication. So far, various chemical compounds that inhibit this conformational conversion have been identified. Here, we report the novel anti-prion activity of SGI-1027 and its meta/meta analog (M/M), previously known only as potent inhibitors of DNA methyltransferases (DNMTs). These compounds effectively decreased the level of PrP^{Sc} in cultured cells with permanent prion infection, without affecting PrP^C at the transcriptional or translational levels. Furthermore, SGI-1027 prevented effective prion infection of the cells. In a PrP aggregation assay, both SGI-1027 and M/M blocked the formation of misfolded PrP aggregates, implying that binding of these compounds hinders the PrP conversion process. A series of binding and docking analyses demonstrated that both SGI-1027 and M/M directly interacted with the C-terminal globular domain of PrP^C, but only SGI-1027 bound to a specific region of PrP^C with high affinity, which correlates with its potent anti-prion efficacy. Therefore, we report SGI-1027 and related compounds as a novel class of potential anti-prion agents that preferentially function through direct interaction with PrP^C.

KEY WORDS   Prion; DNMT; Therapeutic compounds; PrP^C; Epigenetic regulation

1. Introduction

The accumulation of misfolded prion proteins (PrPs) associated with transmissible spongiform encephalopathies (TSEs), also known as prion diseases, results in neuronal cell death and formation of spongy architecture in the central nervous system[1]. Human prion diseases include Creutzfeldt-Jakob disease (CJD), Gerstmann-Sträussler-Scheinker disease (GSS), familial fatal insomnia (FFI), kuru and variant CJD (vCJD), whereas animal prion diseases include Scrapie in sheep, goats and moufflons, transmissible mink encephalopathy (TME), chronic wasting disease (CWD) in deer, and bovine spongiform encephalopathy (BSE) in cattle[2]. The scrape is the earliest known prion disease found in European farms during the 18th century and

designated as the first member of a new class of neurological disorders known as TSEs[3]. Nowadays, neuroblastoma cell lines generated by infection with scrapie agent are commonly used as human prion disease model systems to understand pathological process and phenomenology in prion disorders, develop advanced diagnostic techniques, and evaluate drug effects[4,5]. Prions composed of misfolded PrPs are infectious and replicated through a mechanism different from bacterial and viral pathogens[6]. Biochemically, PrP misfolding is facilitated by the conformational change of α-helix-rich cellular PrP (PrP^C) to β-sheet-rich scrapie PrP (PrP^{Sc}) followed by the formation of insoluble aggregates of misfolded PrPs[7-9]. Thus, as a treatment strategy, stabilization of PrP^C is critical to block the pathogenic PrP conversion process, despite that the detailed molecular mechanism for the conversion remains unclear.

Recently, several compounds have been reported to effectively remove PrP^{Sc} from prion-infected cells[10, 11]. Congo red, a compound to stain β-amyloid structure and quinacrine, a well-known anti-malarials drug, directly associates with PrP^C and interferes with the conversion of PrP^C to PrP^{Sc}, resulting in elimination of PrP^{Sc} [12,13]. The Chicago sky blue 6B, identified from a fluorescence-based assay screening, has been shown to inhibit Aβ binding and reduce PrP^{Sc} levels[14]. GN8 and its analogues identified from an *in silico*-based drug screen have been shown to interact with PrP^C and stabilize the PrP^C conformation, resulting in efficient inhibition of prion replication[15,16]. In addition, structurally modified compounds, GJP14 and GJP49 derived from GN8, have been shown the anti-prion activity in cell based test *via* direct interaction with PrP^C [17,18]. NPR-053, NPR-056 and BMD42-29 are identified as anti-prion compounds by the structure-based drug screening, which can reduce PrP^{Sc} levels in cultured cells[19,20]. Meanwhile, chloroquine and various phenothiazine derivatives reduce PrP^{Sc} formation *via* direct coupling with PrP^C in prion-infected cells[21]. Particularly, the ring structure derived from the quinoline or acridine interacts with PrP; and chemicals with a homo- or heterocyclic ring structure most effectively remove PrP^{Sc} [22,23]. One typical example is the ring structure of quinacrine, which directly associates with the scaffold-structured C-terminus of PrP^C [23]. Such phenomenon suggests that the ring structure in compound interacting with PrPs may serve as a critical component to determine its anti-prion potency.

SGI-1027, a quinoline-based chemical with a non-nucleoside structure, blocks the transfer of a methyl group from *S*-adenosyl-L-methionine to cytosine[24]. As a selective inhibitor of the DNA methyltransferase (DNMT) family, it decreases DNA methylation in the genome, leading to increased transcription of tumor suppression genes in cancer cells[25]. Aberrant gene expression caused by epigenetic dysregulation is associated with neurodegenerative disorders including prion diseases[26]. Moreover, hypomethylation in the promoter region leads to overexpression of genes for protein aggregation, suggesting that epigenetic regulation could be relevant to disease-associated PrP aggregation[27,28]. Therefore, epigenetic control could be an alternative therapeutic strategy to suppress protein aggregation. Here, we report the discovery of two previously reported DNMT inhibitors, SGI-1027 and its meta/meta analogue (M/M) as novel anti-prion agents that function preferentially through direct interaction with PrP^C to interfere with PrP conversion.

2. Materials and methods

2.1. Chemical synthesis

SGI-1027 was synthesized in a five-step synthetic route (Supporting Information Scheme S1). Reaction of 4-chloroquinoline and ethyl 4-aminobenzoate, followed by hydrolysis with KOH, yielded 4-(quinolin-4-ylamino) benzoic acid (**1**). N^4-(4-Aminophenyl)-6-methylpyrimidine-2,4-diamine (**2**) was generated by the reaction of 2-amino-4-chloro-6-methylpyrimidine and 4-nitroaniline, followed by reduction with stannous chloride dihydrate ($SnCl_2 \cdot 2H_2O$). Condensation of **1** and **2** generated the final product SGI-1027[25]. The intermediates and final product were confirmed by mass spectrometry and by ^1H and ^{13}C NMR. The purity of synthesized SGI-1027 was determined using high-performance liquid chromatography. Commercially available SGI-1027 (Cat#:S7276, Selleckchem, Houston, TX, USA) was also purchased for comparison. The SGI-1027 analogue meta/meta (M/M) was synthesized following the SGI-1027 synthetic route above (Supporting Information Scheme S2) [29].

2.2. Cell culture and chemical treatment

N2a, ScN2a, and SMB cell lines were cultured in Dulbecco's modified Eagle's medium (DMEM) supplemented with 10% fetal bovine serum, 1% penicillin/streptomycin, and 1% GlutaMax (Invitrogen, Carlsbad, CA, USA) and split every five days. The cells were initially seeded at 2% confluency in 10 cm culture dishes. After cells adhered to the dish surface, different concentrations of SGI-1027 and M/M dimethyl sulfoxide (DMSO) solutions were added. Cells were incubated with compounds for five days and harvested for the PrP^{Sc} assay after examination of over 95% confluency.

2.3. Cell-based PrP^{Sc} assay

After a five-day incubation with the compounds, cells were lysed in 1 mL cell lysis buffer (20 mmol/L Tris, pH 8.0; 150 mmol/L NaCl; 0.5% Nonidet P-40; 0.5% sodium deoxycholate), and solubilized lysate was separated from cell debris. Protein in the cell lysate was quantified using a bicinchoninic acid protein assay kit (Pierce, Rockford, IL, USA). Thirty μg of protein without treatment of proteinase K (PK) was loaded into Western blotting to analyze total PrP protein and βIII-tubulin, and 2 mg of cell lysate was incubated with 20 μg/mL PK (Invitrogen) for 1 h at 37 °C to examine PK-resistant PrP^{Sc}. The protein pellet was collected by centrifugation for 1 h at $16,000 \times g$ at 4 °C[30]. For Western blot analysis, monoclonal anti-PrP antibodies 5C6 (gifted from G. Telling, Colorado State University, USA) [31], 6D11 (Biolegend, San Diego, CA, USA) and anti-βIII-tubulin antibody (sc-69879, Santa Cruz, CA, USA) were used. Membranes were developed with ECL Prime Detection Reagents (GE Healthcare, Amersham, UK) in the G:Box Chemi XR5 system (Syngene, Cambridge, UK). The densitometry of PrP^{Sc} bands was analyzed using GeneTools software (Syngene, Cambridge, UK).

2.4. Cell-based prion infectivity assay

A modified cell blot assay was used to evaluate SGI-1027 effect against pathogenic prions infection[32]. N2a cells were seeded in 96-well plates, cultured for 12 h, and exposed to scrapie prion (RML strain)-infected mouse brain homogenate for 96 h together with increasing concentration of SGI-1027. The 90%–100% confluent cells were split at a 1:10 ratio and cultured for an additional five days with SGI-1027. Then, 20,000

3

cells were transferred to 96-well nitrocellulose filter-bottomed plates and incubated for an additional 12 h for adhering to the membrane. The membrane was washed with phosphate buffered saline (PBS) and soaked with lysis buffer (50 mmol/L Tris-Cl, pH 8.0; 150 mmol/L NaCl; 0.5% sodium deoxycholate; 0.5% Triton X-100). The dried membranes were then treated with PK solution (5 µg/mL PK in lysis buffer) for 90 min at 37 °C, washed with PBS, and incubated with 2 mmol/L phenylmethylsulfonyl fluoride (PMSF) for 2 min at room temperature to stop PK digestion. After washing with PBS, the membrane was incubated with denaturing buffer (3 mol/L guanidinium thiocyanate, 10 mmol/L Tris-Cl, pH 8.0) for 10 min and then rinsed three times with water. The membrane was further blocked with 5% skim milk TBS-T for 1 h and incubated with the anti-PrP antibody 5C6 for 1 h. After washing with TBS-T, horseradish peroxidase-conjugated anti-mouse secondary antibody was used to detect signal. The membrane was developed with the ECL system, and densitometry was analyzed using GeneTools software (Syngene, Cambridge, UK).

2.5. MTT assay

To measure the cytotoxicity of SGI-1027 and M/M, ScN2a cells were seeded in a 24-well culture plate and incubated with SGI-1027 and M/M for 5 days. On the final day, 0.5 mg/mL MTT was added to the culture medium, and cells were further incubated for 2 h. After adding 0.05 mol/L HCl-isopropanol, the MTT formazan product was measured at 570 nm with background subtraction at 650 nm using an Infinite M200Pro Multimode Reader (Tecan, Männedorf, Switzerland)[31].

2.6. RT-PCR

RNA was isolated using TRIzol (Invitrogen) from ScN2a cells incubated with 1 µmol/L SGI-1027 and 4 µmol/L M/M for five days. cDNA was synthesized from 1 µg RNA by SuperScript II (Invitrogen). RT-PCR was performed using 1 µL of synthesized cDNA with primers for mouse *Prnp* gene (5′-GGCCAAGGAGGGGGTACCCAT-3′ and 5′-GCTGGATCTCCCGTCGTAATA-3′) and *Gapdh*, a housekeeping gene as the internal control (5′-GTTGTCTCCTGCGACTTCA-3′ and 5′-GGTGGTCCAGGGTTTCTTA-3′).

2.7. Expression and purification of recombinant human PrP (rhPrP)

rhPrP was prepared from *E. coli*. First, the cDNA fragment encoding the C-terminal core of human PrP (90–230) was cloned into pET100/D-TOPO plasmids (Invitrogen). Next, the expression vector was transformed into *E. coli* BL21 Star (DE3, Invitrogen), and the transformed bacterial cells were grown at 37 °C until OD_{600} = 0.5. After adding 1 mmol/L isopropyl β-D-1-thiogalactopyranoside to induce rhPrP expression, bacterial cells were further cultured for an additional 5 h. rhPrP expression was monitored using SDS-polyacrylamide gel electrophoresis. rhPrP was purified as following: bacterial cells were lysed using the CelLytic B lysis reagent (Sigma-Aldrich, St. Louis, MO, USA). Inclusion bodies were then solubilized from the cell lysate using CelLytic IB (Sigma-Aldrich). Ni-NTA agarose affinity chromatography was used to collect the His-tagged rhPrP.[33]

2.8. Circular dichroism (CD) spectrometry of rhPrP

rhPrP was diluted ~0.2 mg/mL in 20 mmol/L sodium acetate (pH5.5) and CD spectra were measured using a

Chirascan circular dichroism spectrometer (Applied Photophysics, Surrey, UK). The spectra were collected from 190 to 260 nm with 1 nm bandwidth and 1 mm path length at 25 °C.

2.9. Synthesis of biotinylated peptides

Biotin-conjugated PrP peptides were chemically synthesized (Biostem, Ansan, Korea). During solid-phase peptide synthesis, the α amino groups were protected with Fmoc and Boc. After synthesis of the crude peptide, the peptide-resin was incubated with cleavage solution for 3 h. The molecular weight of the peptides released from the resin was verified by mass spectrometry and the confirmed peptides were separated using HPLC.

2.10. Surface plasmon resonance (SPR) analysis

SPR analysis was conducted with the ProteOn XPR36 protein interaction array system (Bio-Rad, Hercules, CA, USA). Purified rhPrP and biotinylated peptides were placed on a ProteOn GLH Sensor Chip (Bio-Rad, Hercules, CA, USA) *via* amine coupling and on a ProteOn NLC Sensor Chip (Bio-Rad, Hercules, CA, USA) *via* binding to avidin, respectively, at a density of ~3000 resonance units. SGI-1027 and M/M were diluted with PBS (pH 7.0) and injected into a flow cell at a flow rate of 100 μL/min. Five different concentrations of each compound were injected, and the dissociation phase was monitored. Data were analyzed using ProteOn Manager Software 2.0 with standard Langmuir models to fit kinetic data. The flow cell was washed with 10 mmol/L NaOH or 0.01% Triton X-100 for 30 s before the injection of each new sample. The equilibrium response (Req) value or maximum response value in the sensorgram was divided by the molecular weight to determine the binding response between PrP and the compounds. A high affinity interaction was represented as low K_D or rapid recognition and binding (high K_a). Formation of a stable complex was calculated using the equation $K_D = K_d/K_a$.

2.11. PrP amyloid formation assay (PAFA)

Ten μg rhPrP was reacted in 0.2 mL reaction buffer (PBS [pH 7.0], 0.2 mol/L guanidine hydrochloride and 10 μmol/L thioflavin T [Sigma-Aldrich]). Various concentrations of SGI-1027 and M/M were mixed with the PAFA mixture and incubated at 37 °C for 48 h with continuously shaking at 300 revolutions per min. The formation of rhPrP aggregates was detected by reading the fluorescence of amyloid-bound ThT in a 96-Well Black UniPlateTM Microplate (GE Healthcare, Piscataway, NJ, USA) using an Infinite M200Pro Multimode reader (Tecan, Männedorf, Switzerland).

2.12. Molecular docking analysis

Two compounds were docked to 4KML chain A using SwissDock in the accurate mode with default parameters and ranked based on Cluster and Fullfitness[34,35]. Protein-ligand interactions were analyzed using LIGPLOT[34]. Structures were visualized by UCSF Chimera[36] and Pymol (PyMOL Molecular Graphics System, Version 1.8 Schrödinger, LLC).

2.13. Statistical analysis

A *t*-test method was used for the data analysis. All represented values in multiple trials are the mean±SD and a *P*-value less than 0.05 was considered for significance.

3. Results and discussion

SGI-1027, synthesized in-house from a quinoline-based compound in five steps (Scheme 1), effectively eliminated PrP^{Sc} in ScN2a cells, a neuroblastoma cell line infected with prions. The PrP^{Sc} level gradually decreased as the concentration of SGI-1027 increased till completely eliminated at 0.5 μmol/L (Fig. 1A). The densitometry analysis identified the half-maximal concentration of PrP^{Sc} inhibition (IC$_{50}$) by SGI-1027 at 50 nmol/L (Fig. 1B), indicating its high potency compared with other previously tested anti-prion compounds[21,22,37]. In SMB, a prion‑infected cell line of mesenchymal origin, SGI-1027 effectively eliminated PrP^{Sc}, showing similar IC$_{50}$ value as seen in ScN2a cells (Supporting Information Fig. S1), which further indicated the anti-prion effect of SGI-1027 was not limited to a certain cell type. In contrast, M/M, an SGI-1027 analogue, with four-fold stronger DNMT inhibition potency than SGI-1027[29], eliminated PrP^{Sc} less effectively with the IC$_{50}$ value at 4 μmol/L. M/M only partially removed PrP^{Sc} at 1 μmol/L in ScN2a cells, while SGI-1027 completely eliminated PrP^{Sc} at same concentration (Fig. 1C). Thus, the efficacy of SGI-1027 to eliminate PrP^{Sc} was about 80 times greater than that of M/M (Supporting Information Fig. S2). These results suggest that the molecular basis of the anti-prion activity of SGI-1027 and M/M is more likely independent of their DNMT potency[29].

The molecular basis of prion infection can be explained by the biochemical event associated with the initial conformational change of PrP^{C} in the cell membrane *via* dimerization to the pathogenic PrP^{Sc}, and thus inhibiting this process could possibly reduce prion infection[38]. SGI-1027, shown to inhibit PrP^{Sc} propagation in prion-infected cells, may also prevent prion infection in normal cells. To test our hypothesis, we analyzed the effects of SGI-1027 in a cell-based prion infection assay. We observed that PrP^{Sc} propagation was interrupted in N2a cells inoculated with a scrapie (RML strain) prions at 1 μmol/L SGI-1027 concentration (Fig. 1D). In contrast, N2a cells inoculated with a scrapie and low concentration SGI-1027 or without SGI-1027 treatment were susceptible to prion infection. These results suggest that SGI-1027 can effectively prevent prion infection in normal N2a cells.

Though the anti-cancer therapeutic effects of SGI-1027 and M/M are reported *via* manifesting apoptotic induction in cancer cells[29], in our cytotoxicity studies, most of the ScN2a cells incubated with up to 1 μmol/L SGI-1027 were viable (Supporting Information Fig. S3A and B), and 80% of cells death started from 2 μmol/L concentration. Considering that SGI-1027 completely eliminated PrP^{Sc} at nmol/L concentrations, its anti-prion activity was not associated with induced cell death or proliferative defects. M/M was even less cytotoxic than SGI-1027. Over 90% of cells were viable up to 4 μmol/L, and significant cell death observed at 8 μmol/L (Fig. S3A and B). Thus, our previously observed PrP^{Sc} elimination at 4 μmol/L was not due to the induced ScN2a cell death, either. Clearly, the anti-prion activity of SGI-1027 and M/M was irrelevant to the influences of cell division or apoptosis.

Previous study has shown that SGI-1027 and M/M alter the expression of various genes by inhibiting DNMTs[25,29]. Thus, we investigated the expression of *Prnp*, the gene encoding PrP^{C}, and found that the transcript was unaltered at 1 μmol/L SGI-1027 or 4 μmol/L M/M in ScN2a cells (Supporting Information Fig. S4). In addition, PrP remained as the same level in cells incubated with or without SGI-1027 or M/M (Fig. 1A

6

and C). Thus, both mRNA and protein levels of PrP^C were unaffected by SGI-1027 and M/M, suggesting that PrP^{Sc} elimination from prion-infected cells is irrelevant to their epigenetic control of DNMT family proteins.

The quinoline ring structure on the previously reported anti-prion compounds is crucial for those compounds to interact directly with PrP to reduce PrP^{Sc} level[39-41]. Both SGI-1027 and M/M include a quinoline ring in their structures, and thus their inhibitory effect might be due to direct interaction with PrP. To test their binding with PrP, we first bacterially expressed and purified recombinant human PrP spanning amino acid residues 90–230 (rhPrP) (Supporting Information Fig. S5A), and then used circular dichroism (CD) spectrometry to confirm that the purified rhPrP retained its conformation, with dominant α-helical and low β-sheet content, resembling the native conformation of PrP^C (Fig. S5B). Next, we used surface plasmon resonance (SPR) binding assay with quinacrine, known to bind to the C-terminal domain of PrP^{C} [23], as a positive control. Quinacrine showed rapid association and dissociation with rhPrP, but increasing concentration (2–10 μmol/L) escalated SPR responses without saturation (Fig. 2A), indicating the non-specific interaction with PrP^{C} [42]. We further conducted the SPR analysis on both SGI-1027 and M/M. The sensorgram curve of both compounds showed rapid association to reach equilibrium (Req) and rapid dissociation to return to baseline without delayed flow (Fig. 2A). Moreover, the binding efficiency of both SGI-1027 and M/M were five to six times higher than that of quinacrine. At the same concentration, 2 μmol/L, the binding response values of SGI-1027 and M/M were 70 and 90, respectively, whereas that of quinacrine was 20 (Fig. 2B). More importantly, SGI-1027 showed a saturated binding response with an equilibrium of association and dissociation at 2.5 μmol/L, while M/M showed a proportional increase of binding response to compound concentration without saturation, similar to that of quinacrine (Fig. 2A). Therefore, though both compounds interacted with rhPrP, their interaction modes were not identical despite their high interaction affinity. The SPR results suggested that SGI-1027 specifically interacted with a certain region of PrP^C in a binding manner different from the physical adherence of M/M and quinacrine in nonspecific manner[42]. The interaction of both laboratory-synthesized and commercially purchased SGI-1027 to rhPrP were identical in SPR binding assay (Fig. 2A). Analysis of kinetic data showed that the equilibrium dissociation rate constants (K_D) of SGI-1027 were 1.61 μmol/L for laboratory-synthesized and 2.01 μmol/L for commercially purchased, respectively (Fig. 2B), while the K_D of M/M was 91.1 μmol/L (Supporting Information Fig. S6). Apparently, the binding efficiency of SGI-1027 to rhPrP was 45 times stronger than M/M. In fact, SGI-1027 gave the lowest K_D value among all tested anti-prion compounds showing specific interaction with PrP^C, about 2.4 times better than the previously reported GN8, with a K_D value of 3.9 μmol/L[41,43]. Although Congo red was reported with a K_D value comparable to SGI-1027, it showed non-specific interaction with PrP^C without binding saturation[42], similar as seen in quinacrine and M/M (Fig. 2A). We attribute the better efficiency of SGI-1027 at eliminating PrP^{Sc} from ScN2a cells to its direct and specific interaction with PrP^C (Fig. S2).

NMR and computational simulation studies suggest that N159 at the A-S2 loop and E196 at the B-C loop are necessary for PrP conversion[10]. In the SwissDock simulation analysis of unbiased blind docking, we determined the top-scored predicted binding sites for SGI-1027 and M/M to localize the binding region on

7

PrP^C. The results indicated SGI-1027 interacted with three regions on PrP^C: residues 118–122, 125–131, and 161–163 (Fig. 3A). A previously reported nanobody known to interact with residues 123–125 in the β0-β1 loop, 164–170 in the β2-α2 loop, and 174–185 in the α2-helix of PrP^C stabilizes the PrP^C structure[44], and thus these two compounds, SGI-1027 and M/M, might bind and function similarly as the nanobody in their anti-prion activity. In the LIGPLOT analysis, the 2-amino-6-methylpyridine ring of SGI-1027 formed three hydrogen bonds, interacting with residues H155, N159, and Y162, which occur in a relatively hydrophilic region of PrP^C. The same ring of M/M formed a single hydrogen bond only with N159 (Fig. 3B). Specifically, the quinoline ring of both compounds preferred to interact with a more hydrophobic domain of PrP^C containing multiple residues: L130, H155, Y157, P158, E160, Y162, and H187 (Fig. 3A). The segment of PrP^C spanning residues 90–175 is transformed into a four-stranded β-sheet core organized in a β-helical configuration, and the further downstream C-terminal segment of PrP^C, including two helical regions, α2 and α3, is maintained in PrP^{Sc}[45]. Thus, the hydrogen bonds formed with both compounds probably contribute to PrP^C stabilization, preventing the region spanning residues 90–175 from undergoing conformational changes to multiple β-sheets as seen in PrP^{Sc}. Also, the conserved palindromic motif AGAAAAGA (residues 113–120 of PrP^C) has been reported to play a role in the conversion of PrP^C to PrP^{Sc}[44]. Therefore, the palindromic sequence in PrP^C occupied by SGI-1027 and M/M could no longer function properly to be converted to PrP^{Sc}, which resulted the inhibition of pathogenic prion formation. Similar values of computationally calculated free energy change (ΔG) of SGI-1027 and M/M (–7.51 and –7.59 kJ/mol, respectively) were obtained (Fig. 3C). Further analysis from the binding complex structures suggests that the greater binding affinity of SGI-1027 than M/M is congruent with the increased number of hydrogen bonds between SGI-1027 and PrP^C and consistent with its greater anti-prion activity than M/M in our previous cell-based assay studies (Fig. 3B).

To confirm the simulated docking results for SGI-1027 and M/M, we chemically synthesized biotin-tagged PrP peptides that partially overlapped on both ends and used them to screen the binding sites of compounds in PrP^C (Supporting Information Table S1). In the SPR binding assay, only two peptides, spanning residues 112–146 and 138–172, specifically interacted with SGI-1027 (Table 1). The residue L130 that participated in hydrophobic interaction with SGI-1027 in docking study is present in the peptide spanning residues 112–146. Moreover, the peptide spanning residues 138–172 contains H155, N159, and Y162 for the formation of three hydrogen bonds, as well as H155, Y157, P158, E160, and Y162 for the hydrophobic interaction with SGI-1027 (Fig. 3A and B). Clearly, our studies suggested interaction between SGI-1027 and PrP^C seems to occur in the crucial region changed into a series of β sheets during transformation into PrP^{Sc}. Unlike SGI-1027, M/M interacted with most peptides, except two peptides spanning residues 23–61 and 89–120 (Table 1), which also corresponded to its non-specific interaction with PrP^C in our SPR results (Fig. 2).

These findings above were further confirmed by the competitive studies on both compounds. We investigated the elimination of PrP^{Sc} in ScN2a cells incubated with different concentrations of SGI-1027 (0.01–0.5 μmol/L), and with or without 1 μmol/L M/M. Although we observed marginal enhancement of anti-prion activity when mixing 1 μmol/L M/M, the efficacy to eliminate PrP^{Sc} appeared great dependence on SGI-

1027 rather than M/M (Supporting Information Fig. S7). In the presence of SGI-1027 alone, the crucial region in PrP^C was occupied and stabilized to prevent further conversion into PrP^{Sc}. While in the presence of both SGI-1027 and M/M, M/M with lower affinity, only occupied several other binding sites on PrP^C surface, which resulted almost no enhancement in the overall inhibition. Therefore, we reasoned that the SGI-1027 binding site is more crucial to prevent further conformational change than those non-specific adherences of M/M on PrP^C.

PrP^{Sc}, with its β-sheet-rich structure, is hydrophobic and easily forms various aggregates[46]. Recombinant PrP spontaneously converts to amyloid-like, β-sheet-rich forms at neutral or weakly acidic pH[47]. To test whether the direct interaction of SGI-1027 or M/M hinders the conversion of PrP^C to PrP^{Sc} as seen in the previously reported nanobody[48], we measured the effects of SGI-1027 and M/M on the formation of rhPrP aggregates using the PAFA, which detects ThT-positive oligomeric or amyloid fibrils[49]. rhPrP, with a typical α-helix-rich conformation, was converted and aggregated in 10 h, showing abrupt and exponential generation of aggregates (Fig. 4, red). When SGI-1027 was added in the reaction, the exponential PrP aggregation was delayed and eventually inhibited in a dose-dependent manner (Fig. 4, green, purple, cyan, and dark blue). The biphasic pattern of the ThT-curves in the presence of SGI-1027, showed long lag phase and less steep elongation phase to reach plateau, representing the delayed accumulation and shift to PrP^{Sc} extension from amyloid seed, unlike the drastic extension within short reaction time observed in the control. Therefore, we believed that direct interaction between SGI-1027 and PrP^C at the specific sites stabilized PrP^C, retarding the subsequent oligomeric or amyloid formation and extension[50], delaying the further aggregation[48], and thus prevented its conversion to PrP^{Sc}. At the same concentration, SGI-1027 inhibited the formation of PrP aggregates more strongly than M/M, showing effective suppression of PrP aggregates, based on its delayed lag phase and lower ThT fluorescence value (Supporting Information Fig. S8). These results closely correlate with the higher binding affinity of SGI-1027 to PrP^C *via* three hydrogen bonds (Figs. 2B and 3B) and its greater anti-prion activity in ScN2a cells (Fig. 1).

In summary, we report the potent anti-prion activity of SGI-1027. Through cell-based analysis on PrP^{Sc} level, *in vitro* PrP aggregation assay, *in vitro* binding analysis, and *in silico* docking simulation of SGI-1027 and its analogue M/M, we demonstrate that the anti-prion activity of SGI-1027 is due to its direct, specific, and high-affinity interaction with the critical region of PrP^C, and thus prevent it undergo further conformational conversion into β-sheets in PrP^{Sc}. The potency of SGI-1027 is outstanding among all tested anti-prion compounds showing specific interaction to PrP^C so far. Structural modification of SGI-1027 to further increase its anti-prion activity and reduce its cytotoxicity will be a promising future in the development of potential therapeutic compounds for prion disease.

Acknowledgments

9

References

1   Prusiner SB. Prion diseases and the BSE crisis. *Science* 1997;**278**:245-51.

2   Das AS, Zou WQ. Prions: beyond a single protein. *Clin Microbiol Rev* 2016;**29**:633-58.

3   Zabel MD, Reid C. A brief history of prions. *Pathog Dis* 2015;**73**:ftv087.

4   Race RE, Caughey B, Graham K, Ernst D, Chesebro B. Analyses of frequency of infection, specific infectivity, and prion protein-biosynthesis in Scrapie-infected neuro-blastoma cell clones. *J Virol* 1988;**62**:2845-9.

5   Butler DA, Scott MRD, Bockman JM, Borchelt DR, Taraboulos A, Hsiao KK, et al. Scrapie-infected murine neuro-blastoma cells produce protease-resistant prion proteins. *J Virol* 1988;**62**:1558-64.

6   Cobb NJ, Surewicz WK. Prion diseases and their biochemical mechanisms. *Biochem* 2009;**48**:2574-85.

7   Prusiner SB. Novel proteinaceous infectious particles cause scrapie. *Science* 1982;**216**:136-44.

8   Aguzzi A, Polymenidou M. Mammalian prion biology: one century of evolving concepts. *Cell* 2004;**116**:313-27.

9   Caughey B, Baron GS, Chesebro B, Jeffrey M. Getting a grip on prions: oligomers, amyloids, and pathological membrane interactions. *Annu Rev Biochem* 2009;**78**:177-204.

10   Kuwata K, Nishida N, Matsumoto T, Kamatari YO, Hosokawa-Muto J, Kodama K, et al. Hot spots in prion protein for pathogenic conversion. *Proc Natl Acad Sci U S A* 2007;**104**:11921-6.

11   Ferreira NC, Marques IA, Conceicao WA, Macedo B, Machado CS, Mascarello A, et al. Anti-prion activity of a panel of aromatic chemical compounds: *in vitro* and *in silico* approaches. *PLoS One* 2014;**9**:e84531.

12   Trevitt CR, Collinge J. A systematic review of prion therapeutics in experimental models. *Brain* 2006;**129**:2241-65.

13   Cashman NR, Caughey B. Prion diseases—close to effective therapy?. *Nat Rev Drug Discov* 2004;**3**:874-84.

14   Risse E, Nicoll AJ, Taylor WA, Wright D, Badoni M, Yang XF, et al. Identification of a compound that disrupts binding of amyloid-beta to the prion protein using a novel fluorescence-based assay. *J Biol Chem* 2015;**290**:17020-8.

15   Kuwata K, Nishida N, Matsumoto T, Kamatari YO, Hosokawa-Muto J, Kodama K, et al. Hot spots in prion protein for pathogenic conversion. *Proc Natl Acad Sci U S A* 2007;**104**:11921-6.

16   Kimura T, Hosokawa-Muto J, Kamatari YO, Kuwata K. Synthesis of GN8 derivatives and evaluation

of their antiprion activity in TSE-infected cells. *Bioorg Med Chem Lett* 2011;**21**:1502-7.

17   Hosokawa-Muto J, Kamatari YO, Nakamura HK, Kuwata K. Variety of antiprion compounds discovered through an *in silico* screen based on cellular-form prion protein structure: correlation between antiprion activity and binding affinity. *Antimicrob Agents Chemother* 2009;**53**:765-71.

18   Kimura T, Hosokawa-Muto J, Asami K, Murai T, Kuwata K. Synthesis of 9-substituted 2,3,4,9-tetrahydro-1*H*-carbazole derivatives and evaluation of their anti-prion activity in TSE-infected cells. *Eur J Med Chem* 2011;**46**:5675-9.

19   Ishibashi D, Nakagaki T, Ishikawa T, Atarashi R, Watanabe K, Cruz FA, et al. Structure-based drug discovery for prion disease using a novel binding simulation. *Ebiomedicine* 2016;**9**:238-49.

20   Hyeon JW, Choi J, Kim SY, Govindaraj RG, Hwang KJ, Lee YS, et al. Discovery of novel anti-prion compounds using *in silico* and *in vitro* approaches. *Scientific reports* 2015;**5**:14944.

21   Korth C, May BC, Cohen FE, Prusiner SB. Acridine and phenothiazine derivatives as pharmacotherapeutics for prion disease. *Proc Natl Acad Sci U S A* 2001;**98**:9836-41.

22   Doh-Ura K, Iwaki T, Caughey B. Lysosomotropic agents and cysteine protease inhibitors inhibit scrapie-associated prion protein accumulation. *J Virol* 2000;**74**:4894-7.

23   Vogtherr M, Grimme S, Elshorst B, Jacobs DM, Fiebig K, Griesinger C, et al. Antimalarial drug quinacrine binds to C-terminal helix of cellular prion protein. *J Med Chem* 2003;**46**:3563-4.

24   Bestor TH. The DNA methyltransferases of mammals. *Hum Mol Genet* 2000;**9**:2395-402.

25   Datta J, Ghoshal K, Denny WA, Gamage SA, Brooke DG, Phiasivongsa P, et al. A new class of quinoline-based DNA hypomethylating agents reactivates tumor suppressor genes by blocking DNA methyltransferase 1 activity and inducing its degradation. *Cancer Res* 2009;**69**: 4277-85.

26   Qureshi IA, Mehler MF. Developing epigenetic diagnostics and therapeutics for brain disorders. *Trends Mol Med* 2013;**19**:732-41.

27   Urdinguio RG, Sanchez-Mut JV, Esteller M. Epigenetic mechanisms in neurological diseases: genes, syndromes, and therapies. *Lancet Neurol* 2009;**8**:1056-72.

28   Saijo E, Kang HE, Bian J, Bowling KG, Browning S, Kim S, et al. Epigenetic dominance of prion conformers. *PLoS Pathog* 2013;**9**:e1003692.

29   Valente S, Liu Y, Schnekenburger M, Zwergel C, Cosconati S, Gros C, et al. Selective non-nucleoside inhibitors of human DNA methyltransferases active in cancer including in cancer stem cells. *J Med Chem* 2014;**57**:701-13.

30   Ryou C, Legname G, Peretz D, Craig JC, Baldwin MA, Prusiner SB. Differential inhibition of prion propagation by enantiomers of quinacrine. *Lab Invest* 2003;**83**:837-43.

31   Kang HE, Weng CC, Saijo E, Saylor V, Bian J, Kim S, et al. Characterization of conformation-dependent prion protein epitopes. *J Biol Chem* 2012;**287**:37219-32.

32   Klohn PC, Stoltze L, Flechsig E, Enari M, Weissmann C. A quantitative, highly sensitive cell-based infectivity assay for mouse scrapie prions. *Proc Natl Acad Sci U S A* 2003;**100**:11666-71.

33   Kim DH, Lee HM, Ryou C. Evaluation of infective property of recombinant prion protein amyloids in cultured cells overexpressing cellular prion protein. *J Korean Med Sci* 2014;**29**: 1604-9.

34   Wallace AC, Laskowski RA, Thornton JM. LIGPLOT: a program to generate schematic diagrams of protein-ligand interactions. *Protein Eng* 1995;**8**:127-34.

35   Grosdidier A, Zoete V, Michielin O. Fast docking using the CHARMM force field with EADock DSS. *J Comput Chem* 2011;**32**:2149-59.

36   Pettersen EF, Goddard TD, Huang CC, Couch GS, Greenblatt DM, Meng EC, et al. UCSF chimera—a visualization system for exploratory research and analysis. *J Comput Chem* 2004;**25**:1605-12.

37   Barreca ML, Iraci N, Biggi S, Cecchetti V, Biasini E. Pharmacological agents targeting the cellular prion protein. *Pathogens* 2018;**7**:27.

38   Mallucci G, Collinge J. Rational targeting for prion therapeutics. *Nat Rev Neurosc* 2005;**6**:23-34.

39   Murakami-Kubo I, Doh-Ura K, Ishikawa K, Kawatake S, Sasaki K, Kira J, et al. Quinoline derivatives are therapeutic candidates for transmissible spongiform encephalopathies. *J Virol* 2004;**78**:1281-8.

40   Kocisko DA, Baron GS, Rubenstein R, Chen J, Kuizon S, Caughey B. New inhibitors of scrapie-associated prion protein formation in a library of 2000 drugs and natural products. *J Virol* 2003;**77**:10288-94.

41   Hosokawa-Muto J, Kamatari YO, Nakamura HK, Kuwata K. Variety of antiprion compounds discovered through an *in silico* screen based on cellular-form prion protein structure: correlation between antiprion activity and binding affinity. *Antimicrob Agents Chemother* 2009;**53**:765-71.

42   Kamatari YO, Hayano Y, Yamaguchi K, Hosokawa-Muto J, Kuwata K. Characterizing antiprion compounds based on their binding properties to prion proteins: implications as medical chaperones. *Protein Sci* 2013;**22**:22-34.

43   Kawatake S, Nishimura Y, Sakaguchi S, Iwaki T, Doh-ura K. Surface plasmon resonance analysis for the screening of anti-prion compounds. *Biol Pharm Bul* 2006;**29**:927-32.

44   Abskharon RN, Giachin G, Wohlkonig A, Soror SH, Pardon E, Legname G, et al. Probing the *N*-terminal *β*-sheet conversion in the crystal structure of the human prion protein bound to a nanobody. *J Am Chem Soc* 2014;**136**:937-44.

45   Wille H, Bian W, McDonald M, Kendall A, Colby DW, Bloch L, et al. Natural and synthetic prion structure from X-ray fiber diffraction. *Proc Natl Acad Sci U S A* 2009;**106**:16990-5.

46   Lee S, Antony L, Hartmann R, Knaus KJ, Surewicz K, Surewicz WK, et al. Conformational diversity in prion protein variants influences intermolecular *β*-sheet formation. *EMBO J* 2010;**29**:251-62.

47   Baskakov IV. Autocatalytic conversion of recombinant prion proteins displays a species barrier. *J Biol Chem* 2004;**279**:7671-7.

48   Abskharon RNN, Giachin G, Wohlkonig A, Soror SH, Pardon E, Legname G, et al. Probing the *N*-terminal *β*-Sheet conversion in the crystal structure of the human prion protein bound to a nanobody. *J*

Am Chem Soc 2014;**136**:937-44.

49   Colby DW, Zhang Q, Wang S, Groth D, Legname G, Riesner D, et al. Prion detection by an amyloid
      seeding assay. *Proc Natl Acad Sci U S A* 2007;**104**:20914-9.

50   Stohr J, Weinmann N, Wille H, Kaimann T, Nagel-Steger L, Birkmann E, et al. Mechanisms of prion
      protein assembly into amyloid. *Proc Natl Acad Sci U S A* 2008;**105**:2409-14.

Figure captions

Figure 1 Anti-prion activity of the DNMT inhibitor SGI-1027. (A) Western blots to measure elimination of PrP^{Sc} by SGI-1027 from ScN2a cells. (B) Densitometry analysis of PrP^{Sc} bands. The average PrP^{Sc} levels and error bars represent the means and standard deviations obtained from the analysis performed with three independent western blots. (C) Comparison of the PrP^{Sc} elimination effect of 1 μmol/L of SGI-1027 and M/M. DMSO was used as a vehicle and the PrP^{Sc} level of vehicle-treated sample represents the control. (D) Efficacy of SGI-1027 in preventing prion infection. N2a cells cultured without prion inoculum were used as a control for infection (No). For efficacy measurement, N2a cells inoculated with prions but not incubated with SGI-1027 were used as a positive control and ScN2a cells without SGI-1027 incubation were used as a negative control. The efficacy of SGI-1027 in preventing prion infection was measured as the ratio of PrP with and without protease digestion (+PK/–PK) by densitometric quantification of the cell blot. Error bars are mean±SD of three independent trials.

Figure 2 SPR analysis of direct interaction between the DNMT inhibitors and rhPrP. (A) The sensorgram curves derived from the interactions of immobilized rhPrP with commercially purchased (C) and laboratory-synthesized (L) SGI-1027 and its analog M/M. Interaction of rhPrP with quinacrine was used as a positive control. (B) Analysis of kinetic data for the equilibrium dissociation rate constants (K_D) of tested compounds. Analysis was performed under various concentrations of each compound: 0, 1.25, 2.5, 5, 10, and 20 μmol/L. All SPR data analysis and correction was performed through the use of intuitive software wizards in ProteOn Manager Software.

Figure 3 Computational analysis of the binding domain of PrP^C with SGI-1027 and M/M. (A) Surface representation of PrP^C to show the compound binding pocket on structured region of human PrP^C. Red, acidic or negatively charged region; blue, basic or positively charged region; white, neutral region. (B) Predicted binding mode of PrP^C (pink, ribbon) with SGI-1027 (cyan, stick) and M/M (green, stick). Detailed analysis of the interaction shows residues of PrP^C for compounds with a stick representation. Hydrogen bond: yellow dash. (C) Binding parameters predicted by SwissDock for PrP^C interaction with SGI-1027 and M/M.

Figure 4 Inhibitory effect of SGI-1027 on PrP aggregate formation. Dose-dependent inhibition of SGI-1027 on aggregation of rhPrP in PAFA reaction was plotted. Con, PAFA without rhPrP (blue). Numbers represent the concentration of SGI-1027 mixed for each PAFA reaction.
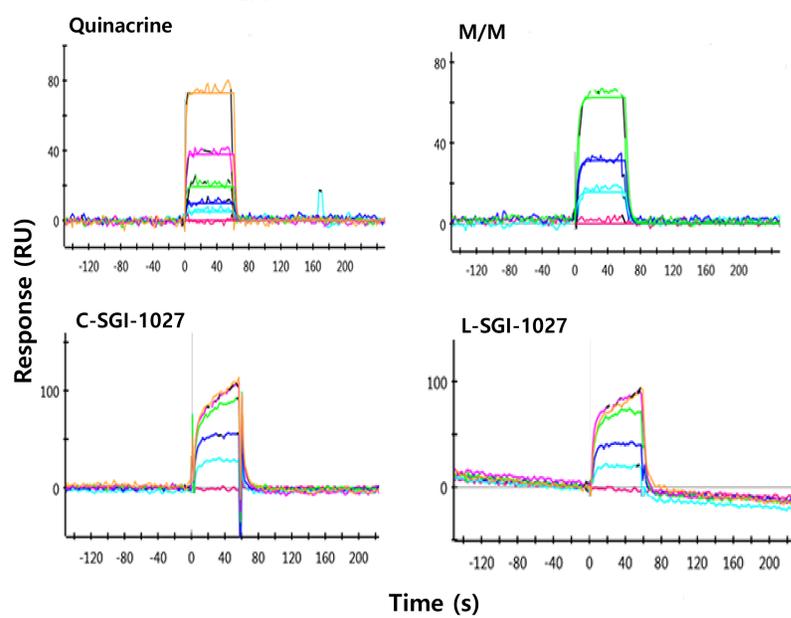
Table 1 Interactions of PrP peptides with laboratory-made (L-) and purchased (C-) SGI-1027 and M/M.

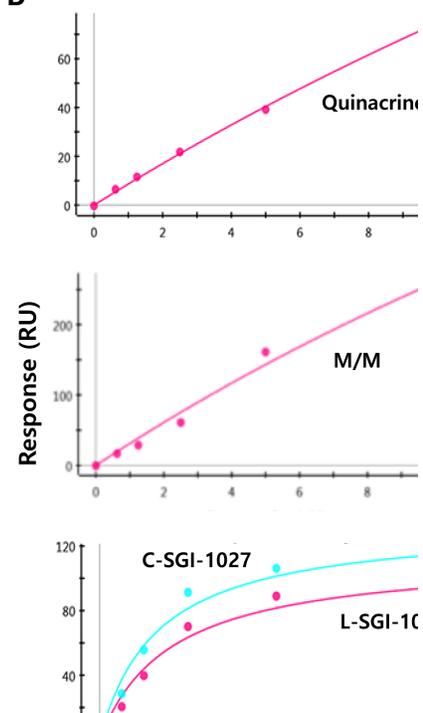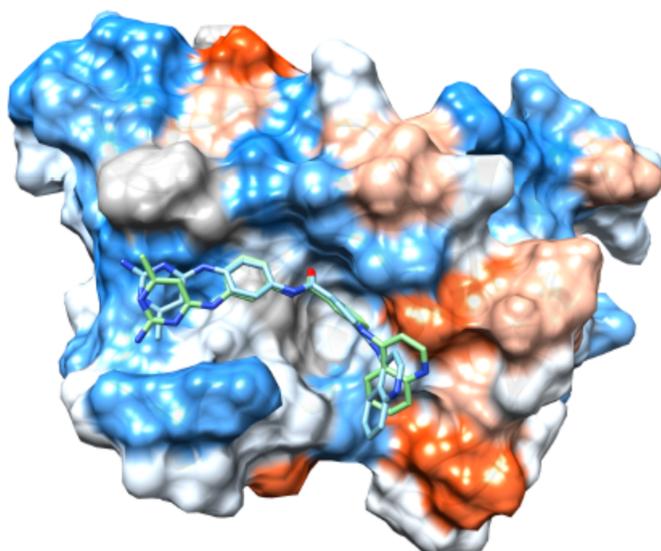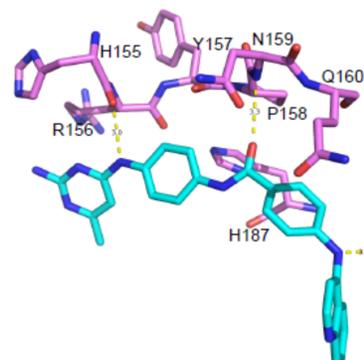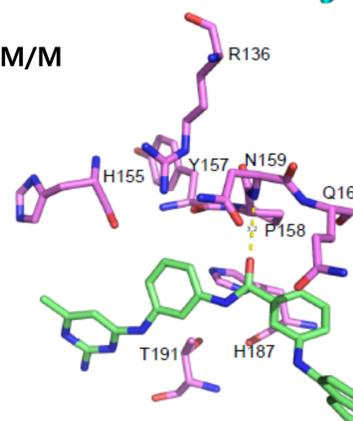| Peptide	Quinacrine	L-SGI1027	C-SGI1027	M/M
23–61	X	X	X	X
57–91	O	X	X	O
89–120	X	X	X	X
112–146	O	O	O	O
128–159	X	X	X	O
138–172	O	O	O	O
157–193	O	X	X	O
169–203	X	X	X	O
193–231	O	X	X	O

O, binding; X, no binding.

A

Quinacrine

M/M

C-SGI-1027

L-SGI-1027

Response (RU)

Time (s)

B

Quinacrine

Response (RU)

M/M
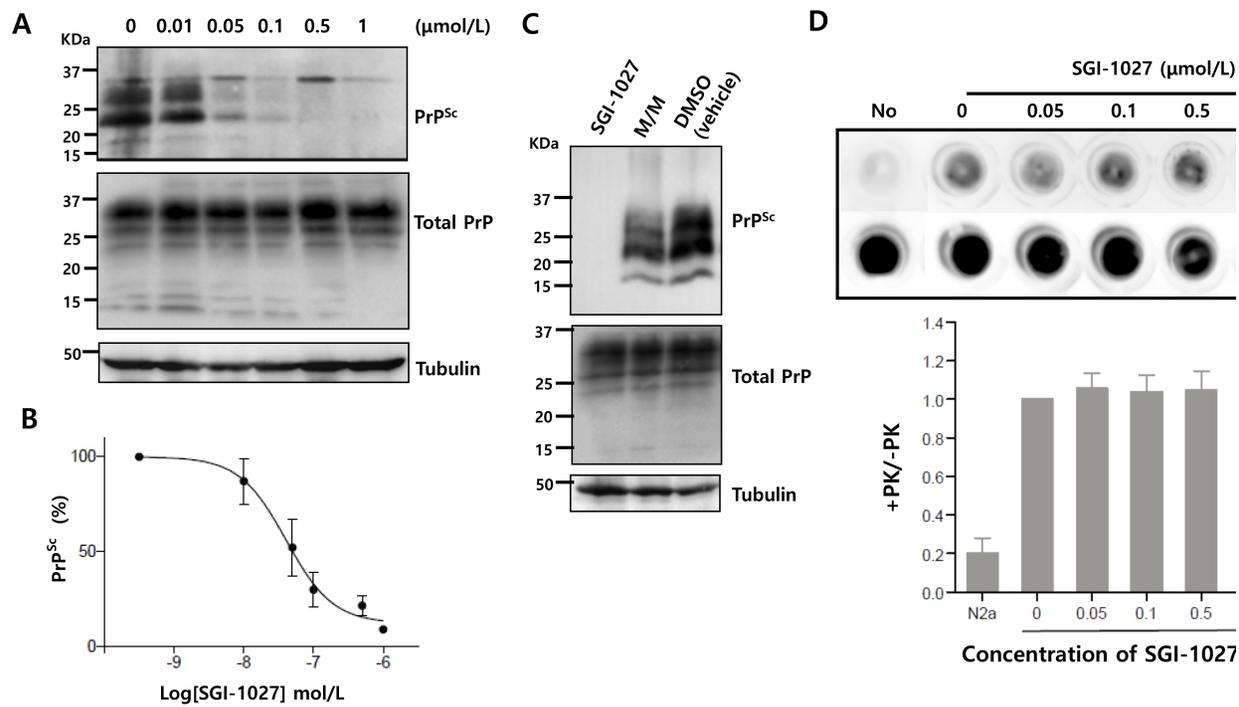
C-SGI-1027

L-SGI-10

A

B SGI-1027

M/M

C

Compound	Highest fitness score	ΔG (KJ/mol)
SGI-1027	683.47	-7.51
M/M	693.98	-7.59